Research

Electrochemical characterization of vascular bare-metal stents. A novel approach modifying the mini-cell system.

Moritz Hertel[1], Michael Laule[2], Spiros Zinelis[3], Sandra Maria Imiolczyk[4],Wolf-Dieter Mueller[5]

[1]Charité Centre 3, Department of Oral Medicine, Dental Radiology and Oral Surgery, Charité UniversitätsmedizinBerlin, Aßmannshauser Str. 4-6, 14197 Berlin, Germany, moritz.hertel@charite.de

[2]Charité Centre 11, Department of Cardiology and Angiology, Cardiac Catheterization Laboratory, Charité Universitätsmedizin Berlin, Charitéplatz 1, 10117 Berlin, Germany, michael.laule@charite.de

[3]Department of Biomaterials, School of Dentistry, National and Kapodistrian University of Athens, 2 Thivon Street, 115 27 Goudi, Athens, Greece, szinelis@dent.uoa.gr

[4]Dörfer Orthodontics Potsdam Sterncenter, Nuthestr. 8, 14480 Potsdam, Germany, sandra.maria.imiolczyk0@gmail.com

[5]Charité Centre 3, Department of Dental Materials and Biomaterial Research, Charité Universitätsmedizin Berlin, Aßmannshauser Str. 4-6, 14197 Berlin, Germany, wolf-dieter.mueller@charite.de

CORRESPONDENCE AUTHOR: Dr. Moritz Hertel
Address: Charité Centre 3, Department of Oral Medicine, Dental Radiology and Oral Surgery (head: Univ.-Prof. Dr. A. M. Schmidt-Westhausen)**,** Charité Universitätsmedizin Berlin**,** Aßmannshauser Str. 4-6**,** 14197 Berlin**,** Germany; phone: +49 (0)30 450 562 692; fax: +49 (0)30 450 562 922**;**
E-mail: moritz.hertel@charite.de

CONFLICTS OF INTEREST
There are no conflicts of interest for any of the authors.

ABSTRACT:
Electrochemical characterization of stents can be seen as a key to assessing their biocompatibility. The aim of the present study was to investigate the electrochemical properties of bare-metal stent surfaces. The mini-cell system (MCS) was modified to record open circuit potential (OCP), cyclic voltammetry (CV) and electrochemical impedance spectroscopy (EIS) on NiTi, FeCrNi and CoCr stents using 1%NaCl, PBS and serum. Surfaces were examined by scanning electron microscopy (SEM) and energy-dispersive X-ray microanalysis (EDX) before and after electrochemical testing. CV showed passivity breakdown of FeCrNi and CoCr in 1%NaCl. Corrosion properties were inhomogeneous. Several surfaces of FeCrNi showed progressive activation and passivity breakdown while pitting was detected by SEM. EDX showed a decrease in Fe, Cr and Ni and an excessive presence of Cl. Corrosion rates (v_{corr}) were partially significantly different between the examined materials and electrolytes (e.g. using 1%NaCl: v_{corr}[FeCrNi]=$2.08 \times 10^{-2} \pm 1.14 \times 10^{-2}$µm/y vs. [NiTi]=$9.41 \times 10^{-3} \pm 1.87 \times 10^{-3}$µm/y; $p < 0.001$). EIS circuit diagrams indicated oxide films on passivated metal surfaces. The modified MCS is promising to assess the biocompatibility of stents via electrochemical analytics. Overall, the v_{corr} of all stents were below the required limit values.

INTRODUCTION

In the case of metals and alloys, biologic response predominately depends on their corrosion properties. Electrochemical characterization can therefore be seen as a key to assessing and controlling their biocompatibility. Related to the high number of annually implanted stents, the lack of data on biocompatibility of the applied materials has been criticized[1]. Overall, adverse effects of stent corrosion have been summarized as tissue reaction, toxicity and mechanical degradation [2]. Several investigations on corrosion resistance of metallic stents or stent materials have been carried out, although the methods are rather inhomogeneous, thereby diminishing comparability. Retrieval analysis studies have been performed to

microscopically identify surface alterations associated with corrosion under biological conditions [3]. Immersion testing was performed to investigate the corrosion properties of stents or stent materials [4], and has frequently been combined with other analysis techniques, such as open circuit potential (OCP) measurements, cyclic voltammetry (CV), electrochemical impedance spectroscopy (EIS) and X-ray photoelectron spectroscopy (XPS) [5-12]. Applications of *in vitro* corrosion analyses include the characterization of surface modifications [9,11,13,14], coatings [5,8,10,12,15,16] and new materials [6,17,18]. *In vivo* OCP measurements have been performed in dogs [19] and humans [20]. The majority of the studies found that the surface features crucially influence corrosion resistance. In this regard, the mini-cell system (MCS) is a promising approach as it enables a variety of electrochemical analysis techniques on micro surfaces [21]. The aim of the present study was to investigate the electrochemical properties of different stents, modifying the MCS to match the arising requirements: first of all, the study intended to characterize the surface´s electrochemical properties as its corrosion resistance has been described as having a major impact on biocompatibility [19]. Furthermore, the aim was to investigate stents in a final deployed form and finished condition as all steps in manufacturing potentially influence corrosion properties [22]. Additionally, multi-focal and spotty examination was intended to enable the detection of inhomogeneities as they have been described to enhance corrosion [23]. Hereupon, immersion testing appears to be inadequate. Foregone electrochemical testing applied either complete wetting of stents [24] or extended measuring surfaces on specimens ranging between 0.25 cm^2 [25] and 4.51 cm^2 [26]. Small measuring surfaces are favourable as inhomogeneities are more unlikely to be detected the larger the measuring surface is. Thus far, the size of the MCS working electrode (WE) has been 0.005 cm^2, so resizing was necessary. As local environmental features have been described to influence the electrochemical behaviour of biomaterials, different physiological media were applied. Assumedly, *in vivo* conditions will be better simulated using body fluids. Since the interpretation of the retrieved results is complicated by their complex composition, it was of particular interest to investigate the extent of differences in corrosion properties if simpler electrolytes are applied. Dilatable stents were analyzed prior to and after dilation to assess if electrochemical properties were influenced by mechanical deformation. It was hypothesized that OCP measurements, CV and EIS

on NiTi, FeCrNi and CoCr stents using 1% NaCl, PBS and human serum would allow for electrochemical distinction of the investigated materials and electrolytes. It was assumed that inhomogeneities within the stents are detectable. Furthermore, it was hypothesized that results indicating corrosion can be confirmed by scanning electron microscopy (SEM) and energy-dispersive X-ray microanalysis (EDX).

EXPERIMENTAL SECTION
Stents and Electrolytes
Three different non-restorable bare-metal stent systems made out of the most frequently used base metal alloys [27,28] were selected: one peripheral self-expanding NiTi memory alloy stent (DynaLink, Guidant, Gießen, Germany) and two balloon-dilatable coronary stents made from FeCrNi (316L stainless steel) (Coroflex, B. Braun, Melsungen, Germany) and CoCr (Coroflex Blue, B. Braun, Melsungen, Germany). Sodium chlorine (1%NaCl), phosphate buffered saline (Dulbecco's PBS without Ca^{2+} and Mg^{2+}, Biochrom, Berlin, Germany) and human serum (PAN-Biotech, Aidenbach, Germany) served as electrolytes.

MCS Modification and Electrochemical Analysis
A detailed description of the MCS and its previous use can be retrieved from the recent literature[29]. To downsize the measuring surface, and hence the working electrode (WE), a pipette tip with a diameter of 0.98 mm^2 was coupled to the MCS resulting in a reduction of approximately 80%. The resulting severely impaired signal-to-noise ratio was improved through grounding of the whole experimental setup in several pre-trials. Saturated calomel (Hg_2Cl_2 (SCE)) and a platinum wire were used as the reference electrode (RE) and the counter electrode (CE). The laboratory unit was supplemented with a reflected-light microscope to allow performing experiments at a 50x magnification to ensure sufficient electrolyte wetting and a standardized WE area. All analyses were carried out applying direct contact mode. Electrolyte leakage was prevented by implementing an aspiration mechanism consisting of a syringe coupled with a polyethylene hose which was connected to the MCS. Thus, a vacuum could be created, if necessary. The MCS was coupled to a potentiostatic (PGZ-402, Radiometer Analytical SAS, Villeurbanne Cedex, and France). Analysis setup and data recording were performed using the software Volta Master 4 (Radiometer Analytical SAS, Villeurbanne Cedex, and France). OCP, CV and EIS were subsequently conducted at room temperature. Three measurements per alloy,

electrolyte and dilation status were performed, as suggested for electrochemical analysis [30]. As a result, nine measuring points were analyzed on the self-expanding NiTi stent and 18 points were examined on each of the dilatable FeCrNi and CoCr stents. The analyses of FeCrNi and CoCr prior to dilation were carried out first. After balloon dilation by applying the parameters determined by the manufacturer, measurements were performed in post-dilation status.

OCP: Initially, the potential between WE and RE was measured at open circuit. All data recorded over each second was averaged. As extended measuring time lead to inevitable electrolyte leakage in several pre-trials, OCP recording time was limited to 240 seconds.

CV: Following OCP measurement, the net current density (i [A/cm^2]) as a function of the shifting WE potential (E [V] vs. SCE) was recorded. Cyclic polarization from -1.2 V to +1.5 V, and reversely, was performed over five cycles with a scan rate of 10 mV/sec. At the end, the circuit was opened at 0 mV to interrupt the current flow. CV data was transferred to Origin Pro 7.5 (Origin Lab Corporation, Northampton, MA, USA). Overlay diagrams of all five cycles recorded per measuring spot were compiled. The zero current potential ($E_{I=0}$ [V] vs. SCE) and the exchange current (I_{corr} [A]) were retrieved from a total of 225 recorded cycles via linear fitting and the exchange current density (i_{corr} [A/cm^2]) was calculated. Corrosion rate (v_{corr} [µm/year]) was computed according to equations 1 and 2.

Eq.1: calculation of corrosion rate per annum (v_{corr} [µm/year]) (F = Faraday's constant= 96500 A * sec/mol, M = molar mass [kg/mol], z = atomic number, ρ = specific gravity [kg/cm^3]).

$$v_{corr} = i_{corr} * \frac{1}{F} * \frac{M}{z*\rho} * 3600\ \text{sec} * 24\,h * 365\,d$$

Eq.2: calculation of the term M_{total} / z_{total} * ρ_{total} for multiple alloying elements (x = atomic percent [at%]

$$\frac{x_{total} * M_{total}}{z_{total} * \rho_{total}} = \frac{x_1 * M_1}{z_1 * \rho_1} + \frac{x_2 * M_2}{z_2 * \rho_2} + \frac{x_3 * M_3}{z_3 * \rho_3}$$

EIS: Electrochemical impedance spectroscopy was performed to investigate the surfaces previously polarized using CV. Prior to EIS, the resting potential was automatically measured independent from the OCP. Phase angle (Φ [°]) was recorded at three frequency ranges (100 mHz – 17.875 Hz, 1 Hz – 1 kHz and 1 kHz – 100 kHz) applying 10 mV amplitude. The electrical impedance (Z [Ω*cm^2]) was calculated. Subsequently, Nyquist ($Z_{imaginary}$ vs. Z_{real}), Bode 1 (Z_{total} and Φ vs. logFreq (frequency)) and Bode 2 plots (C (capacity) vs. logFreq (frequency))of all measuring spots were compiled. Computer-aided fitting (Zview 3.0, Scribner Associates Inc., Southern Pines, NC, USA) was performed to assign circuit diagrams. The circuit providing the best fit was used to simulate its parameters.

SEM and EDX-Analysis
SEM and EDX were performed on one typical surface before and after electrochemical analysis per stent and electrolyte, so twelve analyses were carried out in total. Selection of spots was performed purposefully, preferring electrochemically instable sections based on CV results. Micro-morphological examination was performed recording secondary (SEI) and backscatter electron images (BEI) at variable magnification (Quanta 200, FEI, Hillsboro, OR, USA). A silicon (lithium) detector (Sapphire, EDAX, Mahwah, NJ, USA) with a super ultrathin beryllium window was used for elementary surface analysis. EDX spectra were recorded employing 30 kV accelerating voltage, 110 µA beam current and 200 seconds acquisition time. The quantitative analysis was performed using a dedicate software (Genesis 5.1, EDAX, Mahwah, NJ, USA)applying ZAF (z= atomic number, a= absorption, f= fluorescence) correction methods. Atomic percent ([at%]) were calculated after manual assignment of the obtained line spectra, whereby oxygen and carbon were excluded from the analysis.

Statistical Analysis
Primarily, in electrochemical analytics, every measurement needs to be interpreted singularly. This is due to the peculiarity of corrosion, where singularly measured differences are of potential importance irrespective of statistical significance. Hence, the use of statistical methods was limited to compare the investigated materials and electrolytes. One-way analysis of variance (ANOVA) was performed after Gaussian distribution testing via Shapiro-Wilk test (Origin Pro 7.5, Origin Lab Corporation, Northampton, MA, USA). The significance threshold was determined as a = 0.05.

RESULTS
OCP
Only 15 out of a total of 45 examined surfaces showed steady potentials within the examination period. In serum, the related percentage was the

lowest, whereby no steady OCPs were recorded on CoCr. With the exception of the potential of one surface of FeCrNi using PBS, the OCPs of NiTi and FeCrNi in human serum were more cathodic compared to the other electrolytes (Table 1). Comparison between the materials revealed that FeCrNi was the noblest and CoCr was the least noble in 1%NaCl and PBS, at least within the expressed limitations. In serum, FeCrNi was nobler than NiTi, whereby CoCr could not be assigned.

alloy	electrolyte	E_{OCP} [V] vs. SCE
NiTi	1%NaCl	-0.38
	PBS	-0.37
	serum	-0.63
FeCrNi	1%NaCl	-0.04
		-0.04
		-0.05
	PBS	-0.07
		-0.37
		-0.04
	serum	-0.24
		-0.21
CoCr	1%NaCl	-0.52
		-0.47
	PBS	-0.56
		-0.6

Table 1: Time constant open circuit potentials (E_{OCP}) (n=15).

CV

Comparison between the investigated materials and electrolytes was performed based on the retrieved $E_{i=0}$ and v_{corr} (Figs.1 and 2).
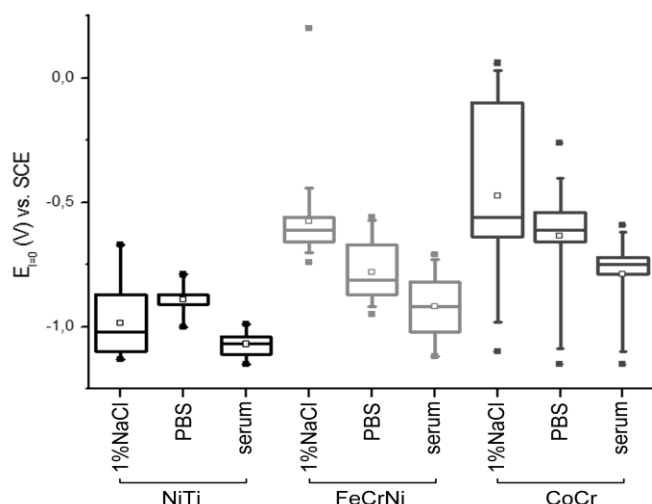

Fig.1: Zero current potentials (EI=0 [V] vs. SCE) of NiTi, FeCrNi and CoCr using 1%NaCl, PBS and serum (99th, 75th, 50th, 25th and 1st percentile). (modified from Hertel [31,32])
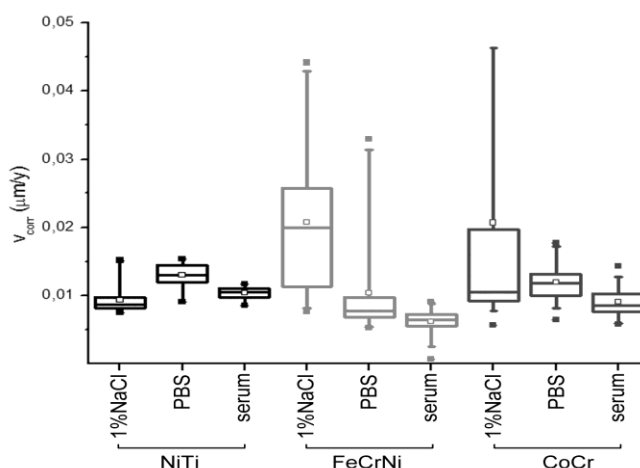

Fig.2: Corrosion rates (vcorr [µm/year]) of NiTi, FeCrNi and CoCr using 1%NaCl, PBS and serum (99th, 75th, 50th, 25th and 1st percentile). Notice that the 99th percentile of CoCr using 1%NaCl was 0.146 µm/year and is not shown to improve the presentation of the y-axis scale. (modified from Hertel [31,32])

Differences between the stents in terms of i_{corr}, $E_{i=0}$ and breakdown potential, as well as the extension of active, transpassive and passive segments were most evident when using 1%NaCl. When utilizing PBS and serum, gradual convergence of the curve shapes was observed (Fig.3). $E_{I=0}$ was significantly different between: NiTi < FeCrNi and NiTi < CoCr using 1%NaCl (both p < 0.001; ANOVA). Furthermore, significantly different $E_{i=0}$ were retrieved from all investigated materials when using PBS and serum (NiTi < FeCrNi < PBS; p < 0.05). Significant differences in v_{corr} were found between: FeCrNi > NiTi utilizing 1%NaCl (p < 0.001). When using PBS, no significant differences were detected. Corrosion rates retrieved utilizing serum differed significantly between all stents (NiTi > CoCr > FeCrNi; p < 0.05) (Table 2).

NiTi: $E_{I=0}$, i_{corr} and v_{corr} of NiTi differed significantly between all applied electrolytes (p < 0.05) (Table 2). However, transpassive segments were overall present within the first and infrequently the second cycle, and breakdown was only seen at potentials over +1.25 V in the following cycles. Extended passivity was observed, accordingly.

FeCrNi: Beween all electrolytes, $E_{I=0}$, i_{corr} and v_{corr} of FeCrNi differed significantly (p < 0.05) (Table 2). Regarding dilation status, v_{corr} was higher post dilation, but significance was only recorded when utilizing serum (5.33 10^{-3}±2.05 10^{-3} vs. 7.23 10^{-2}±1.22 10^{-3} µm/y; p = 0.02). Overall, three types of curve shapes were differentiable (Fig.4): (i) Progressive activation was found in two of six surfaces

examined using 1%NaCl. In addition to a stepwise cathodic shift of $E_{I=0}$, a progressive increase in I was observed in all segments of all cycles. Intermediary, passivity breakdown and subsequent re-passivation were observed followed by a final loss of passivity in the last two cycles. Progressive activation was found in one surface examined with PBS. Nonetheless, passive segments with homogeneousl remained present. Analogous curves were not retrieved from serum. (ii) An alternating increase and decrease in I, especially within the active and transpassive segments, was found for four surfaces using 1%NaCl and in one using PBS. Progressive activation was evident, whereby the course of the cycles differed markedly. (iii) Subsequent deactivation was seen when using PBS (four of six surfaces) and serum. Accordingly, extended passive segments were observed.

Table 2: Average (standard deviation) zero current potentials ($E_{I=0}$), current densities (i_{corr}) and corrosion rates (v_{corr}) retrieved from cyclic voltammetry (standard deviations are given in brackets).

alloy	electrolyte	$E_{I=0}$ [V] vs. SCE	i_{corr} [A/cm^2]	v_{corr} [μm/year]
NiTi	1%NaCl	-0.99 (± 0.13)	$9.64\ 10^{-6}$ (± $1.92\ 10^{-6}$)	$9.41\ 10^{-3}$ (± $1.87\ 10^{-3}$)
	PBS	-0.89 (± 0.05)	$1.33\ 10^{-5}$ (± $1.78\ 10^{-6}$)	$1.30\ 10^{-2}$ (± $1.74\ 10^{-3}$)
	serum	-1.07 (± 0.04)	$1.07\ 10^{-5}$ (± $9.39\ 10^{-7}$)	$1.04\ 10^{-2}$ (± $9.16\ 10^{-4}$)
FeCrNi (total*)	1%NaCl	-0.58 (± 0.17)	$2.51\ 10^{-5}$ (± $1.37\ 10^{-5}$)	$2.08\ 10^{-2}$ (± $1.14\ 10^{-2}$)
	PBS	-0.78 (± 0.11)	$1.26\ 10^{-5}$ (± $8.16\ 10^{-6}$)	$1.04\ 10^{-2}$ (± $6.76\ 10^{-3}$)
	serum	-0.92 (± 0.13)	$7.52\ 10^{-6}$ (± $2.33\ 10^{-6}$)	$6.23\ 10^{-3}$ (± $1.93\ 10^{-3}$)
CoCr (total*)	1%NaCl	-0.47 (± 0.33)	$2.10\ 10^{-5}$ (± $2.79\ 10^{-5}$)	$2.07\ 10^{-2}$ (± $2.74\ 10^{-2}$)
	PBS	-0.64 (± 0.20)	$1.21\ 10^{-5}$ (± $2.56\ 10^{-6}$)	$1.20\ 10^{-2}$ (± $2.52\ 10^{-3}$)
	serum	-0.79 (± 0.14)	$9.20\ 10^{-6}$ (± $2.16\ 10^{-6}$)	$9.06\ 10^{-3}$ (± $2.13\ 10^{-3}$)

* Data on status pre- and post-dilation were pooled.

Table 3: Average (standard deviation) electrolyte resistances (R_S), capacities of the constant phase elements (CPE-T), P-factors (CPE-P) and charge transfer resistances (R_P) retrieved from electrochemical impedance spectroscopy (standard deviations are given in brackets).

alloy	electrolyte	R_S [Ω]	CPE-T [F]	CPE-P	R_P [Ω]
NiTi	1%NaCl	18,424(± 3,921)	$1.16\ 10^{-7}$(± $3.33\ 10^{-8}$)	0.87(± 0.05)	16,041,000(± 4,934,191)
	PBS	121(± 7)	$1.12\ 10^{-4}$(± $3.72\ 10^{-4}$)	0.81(± 0.01)	23,865(± 8,024)
	serum	24,769(± 1,776)	$1.56\ 10^{-7}$(± $4.44\ 10^{-8}$)	0.74(± 0.00)	26,806,666(± 5,666,318)
FeCrNi (total*)	1%NaCl	141(± 24)	$1.30\ 10^{-4}$(± $9.54\ 10^{-5}$)	0.60(± 0.12)	32,413(± 14,693)
	PBS	127(± 39)	$8.73\ 10^{-5}$(± $5.42\ 10^{-5}$)	0.71(± 0.14)	64,794,024(± 91,508,069)
	serum	42,123(± 6,546)	$4.78\ 10^{-8}$(± $3.09\ 10^{-8}$)	0.71(± 0.09)	90,717,167(± 79,916,176)
CoCr (total*)	1%NaCl	17,467(± 3,758)	$9.92\ 10^{-8}$(± $6.16\ 10^{-8}$)	0.80(± 0.03)	29,329,983(± 38,410,495)
	PBS	18,925(± 6,654)	$9.20\ 10^{-8}$(± $6.70\ 10^{-8}$)	0.78(± 0.08)	36,843,700(± 51,490,554)
	serum	36,720(± 11,326)	$8.25\ 10^{-8}$(± $4.85\ 10^{-8}$)	0.74(± 0.06)	8,558,967(± 2,910,708)

CoCr: The obtained $E_{I=0}$ using 1%NaCl, PBS and serum were significantly different (p < 0.05) (Table 2). The highest v_{corr} was recorded when utilizing 1%NaCl followed by PBS, whereas statistical significance was only found between 1%NaCl and serum (p = 0.02) and PBS and serum (p < 0.001). Dilation status did not significantly influence v_{corr}. All retrieved voltammograms corresponded to the described shape types ii and iii. Alternating I (type ii) was ubiquitously observed in 1%NaCl, whereby one half of the surfaces showed progressive extension of the active segments. In contrast, the other half was characterized through extensive passivity and low I. Utilizing PBS, one half of the examined surfaces corresponded to each, type ii and iii, whereby four spots showed singular current peaks within the transpassive segments. Four surfaces analyzed using serum provided decreasing I, whereas progressive active segment extension was observed in two spots.
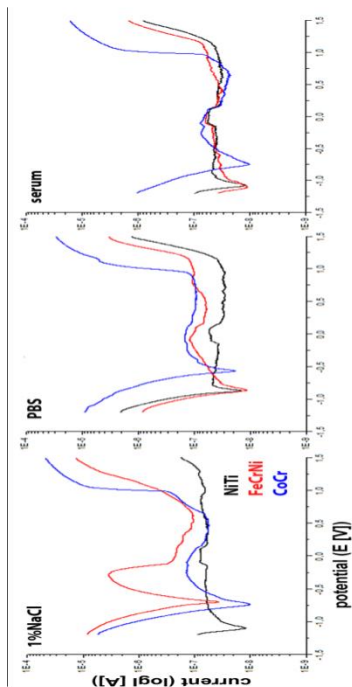
Fig.3: Cyclic voltammograms (cycle 3 of 5) of NiTi, FeCrNi and CoCr (both dilated) using 1%NaCl, PBS and serum. Notice that only the anodic scan is displayed for a better presentation. (modified from Hertel [31,32])
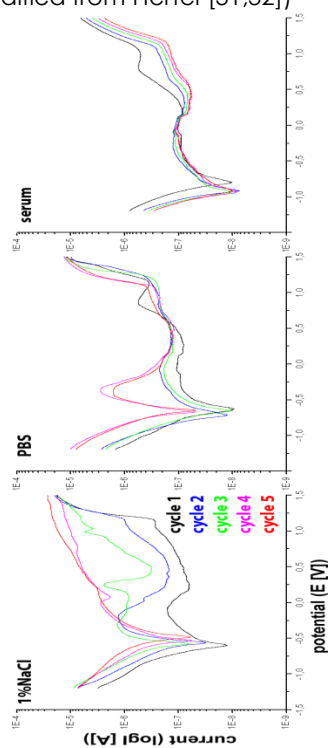

Fig.4: Cyclic voltammograms of FeCrNi (not dilated) using 1%NaCl: total passivity breakdown (type I shape), PBS: alternating current density at progressive activation (type II shape) and serum: extensive passivity (type III shape). Notice that only the anodic scan is displayed for a better presentation. (modified from Hertel [31,32])

EIS

On all 45 surfaces, a time constant was found and a matching circuit diagram could be assigned. This consisted of an omic resistor (R_S [Ω]) series-connected to a constant phase element (CPE) and an additional omic resistor R_P parallel-connected to the CPE (Fig.5).
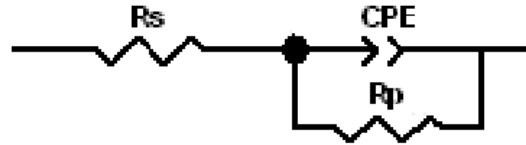

Fig.5: Circuit diagram retrieved from electrochemical impedance spectroscopy data (RS = series-connected omic resistor, RP = parallel-connected omic resistor, CPE = constant phase element).

R_S corresponds to the electric resistance of the electrolyte. The CPE equals a capacitor but its capacity (CPE-T [F]) is not constant, which is expressed by the P-factor (CPE-P) defining the CPE's nature (0 = resistor, 0.5 = Warburg's impedance, 1 = capacitor). Within the circuits, the CPE represents the capacity of the surface's electrochemical double layer or the passive layer, respectively. R_P equals the passive layer's electric resistance or a charge transfer resistance (CTR).
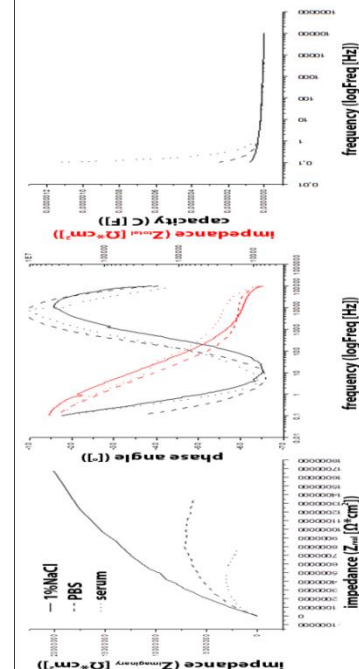

Fig.6: Electrochemical impedance spectroscopy of CoCr (left: Nyquist (Zimaginary vs. Zreal), middle: Bode 1 (Ztotal and Φ vs. log Frequency) and right: Bode 2 plots (Capacity vs. log Frequency)). (modified from Hertel [31,32])

All retrieved plots (Fig.6), circuit diagrams and obtained parameters (Table 3) were characteristic for passivated metal surfaces in contact with aqueous solutions: wide phase angles

were recorded within the Hz range corresponding to capacitive processes. Within the low kHz range (1-10 kHz), Φ drew near 0° in terms of dominance of the omic resistor (Fig.6: Bode 1 plot). Above approximately 10 kHz, the capacity drew near 0 F indicating a dominance of the electrolyte's omic resistance. R_s of serum was significantly higher compared to 1%NaCl (p = 0.006) and PBS (p = 0.007), but only using CoCr. R_p of NiTi applying 1%NaCl was significantly higher than FeCrNi and lower than CoCr (both p = 0.04). No significant differences were found in PBS. Using serum, R_p of CoCr was significantly lower compared to NiTi (p<0.001) and FeCrNi (p = 0.03). Capacities (CPE-T) differed significantly between: FeCrNi > CoCr using 1%NaCl (p = 0.01), NiTi and FeCrNi> CoCr using PBS (p < 0.001 and 0.007) and NiTi > FeCrNi using serum (p < 0.001). Statistically significant differences in P-factor were recorded between: NiTi > CoCr > FeCrNi using 1%NaCl (p = 0.007 and 0.002) and NiTi > FeCrNi using serum (p = 0.04).

SEM and EDX-Analysis

On NiTi, no surfaces showing electrochemical instability were eligible, so SEM and EDX were carried out on each surface first examined per electrolyte. Two surfaces on FeCrNi revealing type i voltamograms (1% NaCl and PBS) and one surface showing a type iii CV (serum) were selected. On CoCr, two measuring spots showing type ii voltammograms were chosen (1% NaCl and PBS). The CV of the selected surface, previously examined utilizing serum, corresponded to type iii. Scanning electron microscopy detected no visible signs of corrosion on NiTi (Fig.7). On the FeCrNi stent, pits and a deep crater were found after using 1%NaCl. The spot analyzed utilizing PBS showed precipitates surrounding a shallow cavity (Fig.8). In contrast, no signs of corrosion were found after using serum. SEM imaging recorded precipitates covering the CoCr surface after applying 1%NaCl and PBS. These were partially chipped off from the surface previously analyzed using PBS. Herein, loss of substance among the grain boundaries was evident (Fig.9). Again, no corrosion correlates were found after applying serum. The atomic surface composition of all analyzed stents was changed after electrochemical testing. Regarding NiTi, changes were only marginal. Within the FeCrNi stent, a decrease of Fe, Cr and Ni was found. The depletion of iron and chromium was highest after using 1%NaCl, where as the highest nickel depletion was found after utilizing PBS (Table 4).The surface of CoCr showed the depletion of Co, in which regard 1%NaCl exceeded PBS. Ni was only diminished after

utilizing PBS. Sodium and chlorine were ubiquitously detected after using 1%NaCl, whereby the percentage of Cl exceeded Na in FeCrNi. Phosphorus was additionally found after applying PBS.

Fig.7: Backscatter electron imaging of NiTi after electrochemical analysis using 1%NaCl and PBS (both: nominal magnification 1200x). (modified from Hertel [31,32])
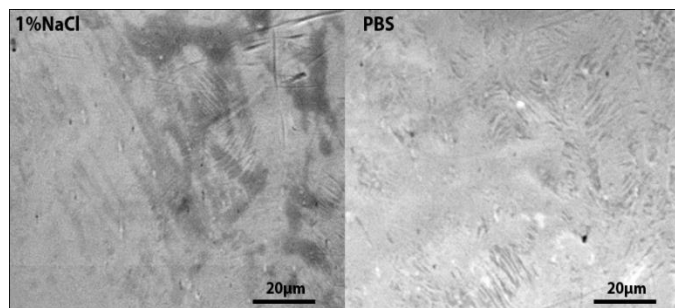

Fig.8: Backscatter electron imaging of FeCrNi after electrochemical analysis using 1%NaCl (left: nominal magnification 500x) and PBS (right: nominal 335x). (modified from Hertel [31,32])
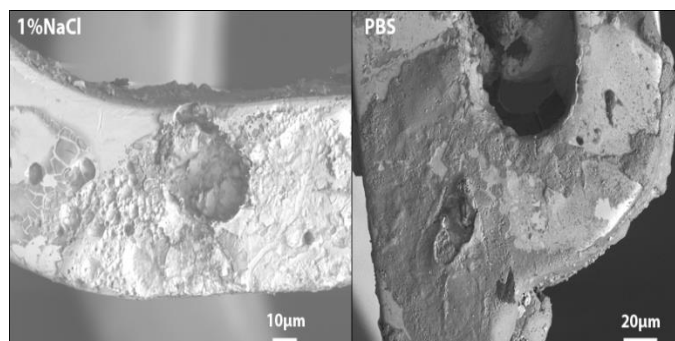

Fig.9: Backscatter electron imaging of CoCr after electrochemical analysis using 1%NaCl (left: nominal magnification 335x) and PBS (right: nominal magnification 1330x). (modified from Hertel [31,32])
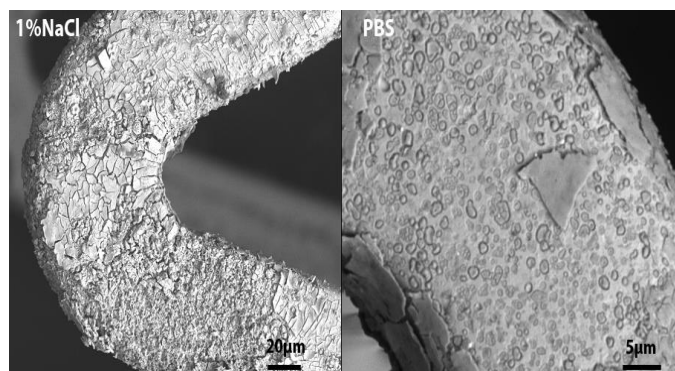
Table 4: Atomic surface composition [at%] of FeCrNi before (t_1) and after (t_2) electrochemical analysis using 1%NaCl, PBS and serum retrieved from energy-dispersive X-ray microanalysis.

element / [at%]		Fe	Cr	Ni	Mn	Mo	Si	Al
t_1	-	62.0	18.7	13.9	1.8	1.7	1.2	0.7
t_2	1%NaCl	23.1	11.1	12.1	12.3	30.6	4.9	6.0
	PBS	44.9	16.5	5.2	3.3	0.9	11.5	15.2
	serum	59.2	16.1	13.8	3.9	0.4	2.2	4.0

Notice that oxygen and carbon were excluded from the analysis.

DISCUSSION

The aim of the present study was to characterize bare-metal stents by sectional electrochemical examination of their surfaces in the finished condition. The presented approach enabled performing all intended analysis methods. The investigated materials and electrolytes were distinguishable regarding parameters retrieved from OCP, CV and EIS. Furthermore, inhomogeneous corrosion properties were recorded within the analyzed stents, as hypothesized. Herein, inhomogeneities were most evident in FeCrNi and CoCr utilizing 1%NaCl. SEM detected signs of corrosion on surfaces showing electrochemical instability based on CV data. Accordingly, EDX recorded changes in the composition of the alloying elements, as assumed. These could be due to ion release or formation of corrosion product layers. An overview of corrosion types of stents can be retrieved from the literature [3]. Pitting corrosion was described as being exceptionally destructive. Electrochemically polished NiTi was found to be resistant to pitting corrosion within polarization of up to +1.0 V [33]. In our study, no signs of pitting were detected, even between -1.2 and +1.5 V. In contrast, FeCrNi analyzed using 1%NaCl showed total passivity breakdown, crater formation as well as surface depletion of Fe, Cr and Ni, corresponding to pitting corrosion. As larger amounts of Cl compared to Na, as well as enrichment of Mn, Mo, Si and Al were detected (Table 4), chlorine salt formation was assumed. The progressive activation found in the CV of CoCr, analyzed utilizing PBS, and was associated with asset erosion and changes in the atomic composition. These results might also be interpreted as pitting corrosion. In addition to the applied analysis methods, reflected-light microscopy performed during CV showed formation of brown stains on FeCrNi and CoCr utilizing 1%NaCl and PBS, which was interpreted as metal oxide deposition. Gas formation was also seen, especially during anodic polarization of FeCrNi using 1%NaCl. The observed effect might due to oxidation of hydroxide ions to oxygen. In general, pitting susceptibility depends on the applied media and is enhanced by its content of chloride ions. The chloride content in 1%NaCl (154 mmol/L) was higher compared to PBS (136.3 mmol/L) and serum (approximately 105 mmol/L). Additionally, phosphate (contained in PBS and serum) and proteins (contained in serum) buffer pH changes, thereby diminishing corrosion. Proteins also might form adsorbent layers limiting charge transfer and ion leakage. Nevertheless, the influence of proteins on corrosion is discussed controversially. Besides pitting, galvanic corrosion may result from inhomogeneities within stents providing a high potential difference. Heterogeneous electrochemical features resulting from the unique shape, geometry and size of stents were postulated before [24]. Firstly, the obtained voltammograms showed a high variability of corrosion susceptibility within the investigated materials. Secondly, the high standard deviation of the parameters retrieved from CV and EIS indicate highly inconsistent electrochemical properties. Nevertheless, the results obtained from EIS need to be interpreted cautiously as impedance spectroscopy was only carried out following CV. The observed heterogeneous response to cyclic polarization might have caused differing surface conditions prior to EIS. This might at least have contributed to the retrieved high standard deviation of EIS parameters. Hence, it has to be emphasized that the obtained EIS data are not comparable to data retrieved by applying immersion conditions.

Metal stents are known to corrode and therefore release ions, which is in accordance with the obtained results. Ion release potentially provides proinflammatory, cytotoxic or fibro-proliferative stimuli. Furthermore, allergenic, carcinogenic or toxic effects, especially of nickel ions, have been frequently discussed [9,34-36]. Corrosion has furthermore been described as a contributor to stent fracture in the periphery [37]. Especially pitting corrosion predisposes to fatigue fracture [3], and shear forces have been discussed to potentially enhance corrosion for their part[26]. The potential impact of mechanical stress was not investigated in

the present study, with the exception of dilation of FeCrNi and CoCr. Only in FeCrNi using serum, v_{corr} was significantly higher after dilation than before. It is likely that the outer surfaces of the struts were not extensively deformed. The corrosion properties of the lateral surfaces were not investigated in the present study, which may be considered in future investigations. Comparing the included stents, their differing strut widths have to be additionally considered as the surface wetted by the electrolyte is proportional to i_{corr} and hence v_{corr}. Effectively the WE, defined as the surface wetted by the electrolyte, varies between the different stents. Nonetheless, corrosion rate was not associated with the strut widths (NiTi > FeCrNi > CoCr). As the WE surface cannot be exactly calculated, it was equated with the surface area of the applied pipette tip in contact with the stent. Even though, the applied pipette tip diameter was still relatively large related to the stent strut dimension, the obtained results were acceptable since the signal-to-noise ratio became lower with a decrease in the WE surface. Future investigations may consider further downsizing of the WE. Furthermore, cyclical mechanical loading as well as flowing electrolytes might help with creating a setup corresponding better to conditions *in vivo*.

For medical devices, a v_{corr} of < 25 µm/y has been defined as being suitable [38]. Corrosions rate of NiTi stents in Hank's solution was reported as 6.47 ± 2.59 * 10^{-6} mm/y (≈ 0.006 µm/y) [24]. Our results are within the same range (0.009 (1%NaCl) to 0.013 µm/y (PBS)). Resistance to corrosion of NiTi and CoCr *in vitro* has been described as being superior to FeCrNi [1,39]. Based on v_{corr}, this was confirmed by our study, at least comparing NiTi and FeCrNi using 1%NaCl. Using serum, the opposite results were retrieved. In this regard, it has to be emphasized that NiTi did not lose passivity in any electrolyte, but FeCrNi and CoCr did, at least in 1%NaCl and PBS. In the present study corrosion rates were determined from the obtained CV curves. It has to be emphasized that extended cyclic polarization is potentially destructive to metal surfaces. Thus, the retrieved v_{corr} do assumedly not correspond to corrosion rates without polarization. Hence, further investigations focusing on corrosion rates or time-dependent processes such as passivity breakdown might consider using only straightforward polarization as well as lower sweep rates. However, v_{corr} of all investigated materials were below the required limit, which in the case of base metal alloys is due to the formation of a passive layer. Its properties forming a boundary layer contacting an aqueous electrolyte were well characterized by the circuit diagrams obtained from EIS. The measured

open circuit potentials of NiTi using 1%NaCl and PBS corresponded well to potentials retrieved *in vivo* [20], but the potentials obtained utilizing serum differed. It can be carefully concluded that serum provides a physiological environment but findings *in vitro* can not necessarily be transferred to conditions *in vivo* as the body environment is electrochemically aggressive to biomaterials. The OCPs retrieved from FeCrNi using serum were within the same range compared to steel wires using Ringer's solution [40]. Potentials previously reported from CoCr wires were different from our results [23], which was likely due to a differing alloy composition.

Electrochemical testing prior to clinical use might help in preventing the adverse effects of stent corrosion including potential contribution to restenosis. Methods applied previously were conducted heterogeneously. Furthermore, sectional assessment of the electrochemical surface properties of implants in the final deployed form and finished condition was not fully accomplished. In this regard, the modified MCS appears to be appropriate within the defined limitations. Technical advancement, including small diameter glass capillaries and low-noise analysis devices, might help in improving electrochemical testing.

It can be concluded that the modified MCS allowed for electrochemical characterization and distinction of different stents using different electrolytes. Overall, NiTi was more resistant to corrosion than FeCrNi and CoCr under the presented conditions. The investigated materials were most susceptible to corrosion when utilizing 1%NaCl, followed by PBS and serum.

CONFLICTS OF INTEREST

REFERENCES

1.Thierry, B.; Tabrizian, M. Biocompatibility and biostability of metallic endovascular implants: State of the art and perspectives. Journal of Endovascular Therapy 2003, 10, 807-824.
2.Mazumder, M.M.; De, S.; Trigwell, S.; Ali, N.; Mazumder, M.K.; Mehta, J.L. Corrosion resistance of polyurethane-coated nitinol cardiovascular stents. Journal of biomaterials science 2003, 14, 1351-1362.
3.Halwani, D.O.; Anderson, P.G.; Brott, B.C.; Anayiotos, A.S.; Lemons, J.E. Surface

characterization of explanted endovascular stents: Evidence of in vivo corrosion. Journal of Biomedical Materials Research Part B-Applied Biomaterials 2010, 95B, 225-238.

4.Hermawan, H.; Alamdari, H.; Mantovani, D.; Dube, D. Iron-manganese: New class of metallic degradable biomaterials prepared by powder metallurgy. Powder Metallurgy 2008, 51, 38-45.

5.Lu, P.; Cao, L.; Liu, Y.; Xu, X.H.; Wu, X.F. Evaluation of magnesium ions release, biocorrosion, and hemocompatibility of mao/plla-modified magnesium alloy we42. Journal of Biomedical Materials Research Part B-Applied Biomaterials 2011, 96B, 101-109.

6.Okazaki, Y.; Goth, E. Metal release from stainless steel, co-cr-mo-ni-fe and ni-ti alloys in vascular implants. Corrosion Science 2008, 50, 3429-3438.

7.O'Brien, B.J.; Stinson, J.S.; Boismier, D.A.; Carroll, W.M. Characterization of an nbtawzr alloy designed for magnetic resonance angiography compatible stents. Biomaterials 2008, 29, 4540-4545.

8.Liu, C.L.; Chu, P.K.; Lin, G.Q.; Qi, M. Anti-corrosion characteristics of nitride-coated aisi 316l stainless steel coronary stents. Surface & Coatings Technology 2006, 201, 2802-2806.

9.Fukushima, O.; Yoneyama, T.; Doi, H.; Hanawa, T. Corrosion resistance and surface characterization of electrolyzed ti-ni alloy. Dental materials journal 2006, 25, 151-160.

10.Maguire, P.D.; McLaughlin, J.A.; Okpalugo, T.I.T.; Lemoine, P.; Papakonstantinou, P.; McAdams, E.T.; Needham, M.; Ogwu, A.A.; Ball, M.; Abbas, G.A. Mechanical stability, corrosion performance and bioresponse of amorphous diamond-like carbon for medical stents and guidewires. Diamond and Related Materials 2005, 14, 1277-1288.

11.O'Brien, B.; Carroll, W.M.; Kelly, M.J. Passivation of nitinol wire for vascular implants - a demonstration of the benefits. Biomaterials 2002, 23, 1739-1748.

12.van Bommel, K.J.C.; Friggeri, A.; Mateman, D.; Geurts, F.A.J.; van Leerdam, K.G.C.; Verboom, W.; van Veggel, F.C.J.M.; Reinhoudt, D.N. Self-assembled monolayers on gold for the fabrication of radioactive stents. Advanced Functional Materials 2001, 11, 140-146.

13.Simka, W.; Kaczmarek, M.; Baron-Wiechec, A.; Nawrat, G.; Marciniak, J.; Zak, J. Electropolishing and passivation of niti shape memory alloy. Electrochimica Acta 2010, 55, 2437-2441.

14.Wang, G.X.; Shen, Y.; Zhang, H.; Quan, X.J.; Yu, Q.S. Influence of surface microroughness by plasma deposition and chemical erosion followed by tio2 coating upon anticoagulation, hydrophilicity, and corrosion resistance of niti alloy stent. Journal of Biomedical Materials Research A 2008, 85, 1096-1102.

15.Holvoet, S.; Horny, P.; Turgeon, S.; Chevallier, P.; Pirezux, J.J.; Mantovani, D. Characterization of film failures by bismuth electrodeposition-application to thin deformed fluorocarbon films for stent applications. Electrochimica Acta 2010, 55, 1042-1050.

16.Levy, Y.; Tal, N.; Tzemach, G.; Weinberger, J.; Domb, A.J.; Mandler, D. Drug-eluting stent with improved durability and controllability properties, obtained via electrocoated adhesive promotion layer. Journal of Biomedical Material Research B Applied Biomaterials 2009, 91, 819-830.

17.Hermawan, H.; Prunama, P.; Dube, D.; Couet, J.; Mantovani, D. Fe-mn alloys for metallic biodegradable stents: Degradation and cell viability studies. Acta biomaterialia 2010, 6, 1852-1860.

18.O'Brien, B.J.; Stinson, J.S.; Larsen, S.R.; Eppihimer, M.J.; Carroll, W.M. A platinum-chromium steel for cardiovascular stents. Biomaterials 2010, 31, 3755-3761.

19.Shih, C.C.; Lin, S.J.; Chung, K.H.; Chen, Y.L.; Su, Y.Y. Increased corrosion resistance of stent materials by converting current surface film of polycrystalline oxide into amorphous oxide. Journal of biomedical materials research 2000, 52, 323-332.

20.Pertile, L.B.; Silva, P.M.; Peccin, V.B.; Peres, R.; Silveira, P.G.; Giacomelli, C.; Giacomelli, F.C.; Fredel, M.C.; Spinelli, A. In vivo human electrochemical properties of a niti-based alloy (nitinol) used for minimally invasive implants. Journal of Biomedical Materials Research A 2009, 89, 1072-1078.

21.Mueller, W.D.; Lucia Nascimento, M.; Lorenzo de Mele, M.F. Critical discussion of the results from different corrosion studies of mg and mg alloys for biomaterial applications. Acta biomaterialia 2010, 6, 1749-1755.

22.Shabalovskaya, S.A.; Tian, H.; Anderegg, J.W.; Schryvers, D.U.; Carroll, W.U.; Van Humbeeck, J. The influence of surface oxides on the distribution and release of nickel from nitinol wires. Biomaterials 2009, 30, 468-477.

23.Su, Y.Y.; Shih, C.C.; Chen, L.C.; Shih, C.M.; Lin, S.J. Heterogeneous surface properties on wallstents. Surface and Interface Analysis 2010, 42, 59-65.

24.Venugopalan, R. Corrosion testing of stents: A novel fixture to hold entire device in deployed form and finish. Journal of biomedical materials research 1999, 48, 829-832.

25.Lee, S.H.; Kim, J.G.; Choi, H.W.; Lee, K.R. Microtensile strain on the corrosion performance of diamond-like carbon coating. Journal of Biomedical Materials Research A 2008, 85, 808-814.

26.Messer, R.L.W.; Mickalonis, J.; Adams, Y.; Tseng, W.Y. Corrosion rates of stainless steel under shear stress measured by a novel parallel-plate flow

chamber. Journal of Biomedical Materials Research Part B-Applied Biomaterials 2006, 76B, 273-280.

27. Weiss, S.; Meissner, A.; Fischer, A. Microstructural changes within similar coronary stents produced from two different austenitic steels. Journal of the mechanical behavior of biomedical materials 2009, 2, 210-216.

28. Silva, R.A.; Silva, I.P.; Rondot, B. Effect of surface treatments on anodic oxide film growth and electrochemical properties of tantalum used for biomedical applications. Journal of biomaterials applications 2006, 21, 93-103.

29. Mueller, W.D.; Schoepf, C.; Nascimento, M.L.; Carvalho, A.C.; Moisel, M.; Schenk, A.; Scholz, F.; Lange, K.P. Electrochemical characterisation of dental alloys: Its possibilities and limitations. Analytical and bioanalytical chemistry 2005, 381, 1520-1525.

30. Müller, W.-D.; Nascimento, L.; Mele, M. Electrochemical assessment of biomaterial surfaces using the mini-cell system. In V Latin American Congress on Biomaterial Engineering, Havanna, Cuba, 2011.

31. Hertel, M. Elektrochemische charakterisierung von stents mit hilfe des adaptierten mini- cell-systems (mcs). Charité - Universitätsmedizin Berlin, Berlin, 2012.

32. Hertel, M. Elektrochemische charakterisierung von stents mit hilfe des adaptierten mini- cell-systems (mcs). Südwestdeutscher Verlag für Hochschulschriften: Saarbrücken, 2014.

33. Pound, B.G. Susceptibility of nitinol to localized corrosion. Journal of Biomedical Materials Research A 2006, 77, 185-191.

34. Shabalovskaya, S.; Anderegg, J.; Rondelli, G.; Vanderlinden, W.; De Feyter, S. Comparative in vitro performances of bare nitinol surfaces. Bio-medical materials and engineering 2008, 18, 1-14.

35. Diaz, M.; Sevilla, P.; Galan, A.M.; Escolar, G.; Engel, E.; Gil, F.J. Evaluation of ion release, cytotoxicity, and platelet adhesion of electrochemical anodized 316 l stainless steel cardiovascular stents. Journal of Biomedical Materials Reserach B Applied Biomaterials 2008, 87, 555-561.

36. Shih, C.C.; Shih, C.M.; Chen, Y.L.; Su, Y.Y.; Shih, J.S.; Kwok, C.F.; Lin, S.J. Growth inhibition of cultured smooth muscle cells by corrosion products of 316 l stainless steel wire. Journal of biomedical materials research 2001, 57, 200-207.

37. Bates, M.C.; Campbell, J.R.; Campbell, J.E. Late complication of stent fragmentation related to the "lever-arm effect". Journal of Endovascular Therapy 2008, 15, 224-230.

38. Liang, C.H.; Guo, L.; Chen, W.; Liu, J.X. Electrochemical behavior of sus316l stainless steel after surface modification. Transactions of Nonferrous Metals Society of China 2003, 13, 398-401.

39. Hanawa, T. Materials for metallic stents. Journal of Artificial Organs 2009, 12, 73-79.

40. Shih, C.C.; Shih, C.M.; Chows, K.Y.; Lin, S.J.; Su, Y.Y. Stability of passivated 316l stainless steel oxide films for cardiovascular stents. Journal of Biomedical Materials Research Part A 2007, 80A, 861-873.